



# รายงานวิจัยฉบับสมบูรณ์

โครงการ: การสร้างแบบจำลองของกระบวนการผลิตชิ้นส่วนคอมโพสิต จากใยเคลือบเมตริกซ์

Modelling of matrix coated fibre composite component manufacturing processes

โดย: ดร. จุฬาลักษณ์ ค้าไม้

ภาควิชาวิศวกรรมการผลิต

คณะวิศวกรรมศาสตร์

สถาบันเทคโนโลยีพระจอมเกล้าพระนครเหนือ

# รายงานวิจัยฉบับสมบูรณ์

โครงการ: การสร้างแบบจำลองของกระบวนการผลิตชิ้นส่วนคอมโพสิต จากใยเคลือบเมตริกซ์

Modelling of matrix coated fibre composite component manufacturing processes

โดย: ดร. จุฬาลักษณ์ ค้าไม้

ภาควิชาวิศวกรรมการผลิต

คณะวิศวกรรมศาสตร์

สถาบันเทคโนโลยีพระจอมเกล้าพระนครเหนือ

สนับสนุนโดยทบวงมหาวิทยาลัย และสำนักกองทุนสนับสนุนการวิจัย

(ความเห็นในรายงานนี้เป็นของผู้วิจัย ทบวงฯ และสกว. ไม่จำเป็นต้องเห็นด้วยเสมอไป)

# กิตติกรรมประกาศ

ผู้วิจัยขอขอบคุณ Dr. Fionn Dunne เป็นอย่างยิ่งที่ให้ความกรุณาเป็น Mentor ของโครงการวิจัยนี้ และให้คำแนะนำและช่วยเหลือตลอดระยะเวลาที่ดำเนินโครงการ รวมถึง Dr. H. X. Peng สำหรับผลการ ทดลองที่นำมาใช้ในการยืนยันความถูกต้องของแบบจำลอง ผู้วิจัยขอขอบคุณภาควิชาวิศวกรรมการผลิต สถาบันเทคโนโลยีพระจอมเกล้าพระนครเหนอ สำหรับสถานที่ในการทำวิจัย และขอขอบคุณสำนักงานกอง ทุนสนับสนุนการวิจัยที่ให้ทุนในการทำวิจัยครั้งนี้

จุฬาลักษณ์ คำไม้

## บทคัดย่อ

ในขณะนี้โลหะคอมโพสิตกำลังได้รับความนิยมอย่างมากในการใช้ทำชิ้นส่วนเกี่ยวกับอากาศยานที่อุณหภูมิสูง โลหะคอมโพสิตสามารถผลิตโดยใช้วิธีใยเคลือบเมตริกซ์ การจำลองการผลิตโลหะคอมโพสิตจากใยเคลือบ เมตริกซ์นั้นจะเชื่อถือได้มากน้อยเพียงใดขึ้นกับการใช้สมการคอนสติติวทีฟที่เหมาะสม ในปัจจุบันมีเพียงไม่กี่ สมการที่ถูกพัฒนาขึ้นมาสำหรับโลหะคอมโพสิตแบบใยเคลือบเมตริกซ์ซึ่งสมการเหล่านี้เป็มสมการเชิง ประจักษ์โดยส่วนใหญ่หรือเป็นสมการที่ใช้สำหรับการเรียงตัวของใยเคลือบเมตริกซ์แบบอาเรย์สี่เหลี่ยมซึ่งเป็น รูปแบบการจัดเรียงตัวที่ไม่ซับซ้อนสำหรับการคำนวณ ในทางปฏิบัตินั้นการเปลี่ยนการจัดเรียงของใยเคลือบ เมตริกซ์ระหว่างกระบวนการเป็นสิ่งที่หลีกเลี่ยงไม่ได้ ถึงแม้ว่าการจัดเรียงตัวในตอนแรกจะเป็นแบบอาเรย์สิ่ เหลี่ยมแต่ใยเคลือบเมตริกซ์มักจะจัดเลียงตัวเองให้อยู่ในรูปแบบที่เสถียรที่สุดนั่นคือมักจะอยู่ในรูปแบบอาเรย์ ในงานวิจัยนี้ได้ทำการพัฒนาสมการคอนสติติวทีฟเชิงกายภาพสำหรับกระบวนการทำให้ความ หนาแน่นเพิ่มขึ้นสำหรับการจัดเรียงตัวแบบอาเรย์หกเหลี่ยม สร้างสมการโดยพิจารณายนิตสำหรับอาเรย์หก เหลี่ยมที่อยู่ภายใต้แรงกดเท่ากันในระนาบ สมการดังกล่าวพัฒนาโดยใช้หลักการแปรผัน สมการคอนสติติว ทีฟที่ได้นี้ได้ถูกพัฒนาต่อเพื่อให้ใช้ได้กับสภาวะความเค้นโดยทั่วไป (ซึ่งเป็นความเค้นหลายแกน) คอนสติติวทีฟนี้ได้ถูกนำไปใช้ร่วมกับโปรแกรมไฟไนต์เอลิเมนต์โดยการคำนวณค่าต่างๆจะอ้างอิงกับทฤษฎี การเสียรูปมากทั้งนี้เพื่อที่จะได้จำลองกระบวนการผลิตในทางปฏิบัติได้ แบบจำลองต้องการทราบตัวแปร เพียงสองตัวคือค่าคงที่ของการคืบของโลหะเคลือบ แบบจำลองได้ถูกตรวจสอบยืนยันความถูกต้องโดยทำ การเปรียบเทียบผลการทำนายกับผลที่ได้จากการทำนายโดยใช้แบบจำลองแบบจุลภาค ผลการจำลองยังได้ ถูกนำไปเปรียบเทียบกับผลการทดลองจริงซึ่งพบว่าเปรียบเทียบกันได้ดี จากผลการจำลองพบว่ากราฟการ ทำให้ความหนาแน่นเพิ่มขึ้นที่ได้จากอาเรย์สี่เหลี่ยมและอาเรย์หกเหลี่ยมนั้นเป็นเหมือนขอบล่างและขอบบน ของพฤติกรรมการเพิ่มขึ้นของหนาแน่นของใยเคลือบเมตริกซ์ภายใต้การกดแบบแกนเดียวในทางปฏิบัติ

คำหลัก: metal matrix composite, constitutive modeling, finite element method

#### **Abstract**

Metal matrix composites are increasingly attractive for high temperature aerospace applications. They can be fabricated using the matrix-coated fibre (MCF) method. Simulations of consolidation of matrix-coated fibre composite rely on the existence of suitable constitutive equations. The few existing constitutive equations for matrix-coated fibre composite consolidation are either largely empirical or developed for square array packing of coated fibres of which the configuration involves less complex calculation. In practical consolidation process, fibre re-arrangement may inevitably occur. Even though the initial fibre arrangement is square array, as consolidation proceeds, stacks of coated fibres are likely to fall into hexagonal array configuration as it is the most stable configuration. This research, therefore, addresses the development of a new physically-based constitutive equations for the densification of MCF hexagonal arrays. Unit cells representing hexagonal array packing of the coated fibres under symmetric in-plane compressive load have firstly been established. The model is based on a variational method. The resulting constitutive equations have subsequently been generalised to multiaxial stress states and implemented into finite element software within a finite deformation framework to enable simulations of practical manufacturing processes. The model requires only two material parameters which are the creep constants of the matrix material. The model has been verified by comparing predicted results with those obtained from independently developed micro-mechanical models. The simulation results have also been compared with experimental results. Good agreement is achieved. The results of simulation suggest that the densification curves for square array and hexagonal array packing effectively provide the lower and upper bounds, respectively for the practical consolidation behaviour of MCFs array under uniaxial constrained compression.

Keywords: metal matrix composite, constitutive modeling, finite element method

#### **Executive Summary**

Project Code: MRG4680083

**Project Title:** Modelling of matrix-coated fibre composite component

manufacturing processes

Investigator: Dr. Julaluk Carmai

Department of Production Engineering , Faculty of Engineering

King Mongkut's Institute of Technology North Bangkok

Email address: jcm@kmitnb.ac.th

Project Period: 1 year and 6 months

Project budget: 190,000.00 Bath

Metal matrix composites are increasingly attractive for high temperature aerospace applications. They can be fabricated using the matrix-coated fibre (MCF) method. Simulations of consolidation of matrix-coated fibre composite rely on the existence of suitable constitutive equations. existing constitutive equations for matrix-coated fibre composite consolidation are either largely empirical or developed for square array packing of coated fibres of which the configuration involves less complex calculation. In practical consolidation process, fibre re-arrangement may inevitably occur. Even though the initial fibre arrangement is square array, as consolidation proceeds, stacks of coated fibres are likely to fall into hexagonal array configuration as it is the most stable configuration. This research, therefore, addresses the development of a new physically-based constitutive equations for the densification of MCF hexagonal arrays. Unit cells representing hexagonal array packing of the coated fibres under symmetric in-plane compressive load have firstly been established. The model is based on a variational method. The resulting constitutive equations have subsequently been generalised to multiaxial stress states and implemented into finite element software within a finite deformation framework to enable simulations of practical manufacturing processes. The model requires only two material parameters which are the creep constants of the matrix material. The model has been verified by comparing predicted results with those obtained from independently developed micro-mechanical models. The simulation results have also been compared with experimental results. Good agreement is achieved. The results of simulation suggest that the densification curves for square array and hexagonal array packing effectively provide the lower and upper bounds, respectively for the practical consolidation behaviour of MCFs array under uniaxial constrained compression.

#### 1. Introduction

The aeroengine is one of the most hostile and demanding environments for any material system. It requires advanced materials with improved specific properties, high temperature capabilities and low density. Continuous ceramic fibre reinforced titanium alloys are being developed for such application. The application of titanium metal matrix composites (Ti-MMCs) is largely envisaged in the compressor section of the aeroengine. They are generally used as local reinforcement in otherwise monolithic material components. Such locally reinforced composite components can be produced by inserting a bundle of continuous fibres, which are pre-coated with the titanium alloy matrix, into recesses machined into components also made from the titanium alloy. The application of pressure at an appropriate temperature causes the consolidation of the composite and also allows the fibre coatings to diffusion bond to the sides of the recess in the component.

The consolidation process is important in determining the properties of the final composite components. Pressure and temperature cycles have to be chosen with care to ensure that all porosity is eliminated, that diffusion bonding between the composite and surrounding monolithic material is complete, and that imposed loading at elevated temperature does not lead to distortion of the finished component. Computer simulation, alternative to costly and time consuming trial and error experiments, can allow the prediction of optimum temperature, pressure and time required to obtain fully dense composite material. It also enables manufacturing process design. Computer simulation, however, relies on the existence of suitable constitutive equations capable of determining the evolution of deformation and porosity in the composite when subjected to any, general stress state. The few existing models for matrix-coated fibre composite consolidation are either largely empirical and rely on parametric finite element studies for their useful application or are unable to provide constitutive equations which explicitly account for matrix-fibre-void systems.

Recently, Carmai and Dunne (2001, 2003) have developed physically based constitutive model for matrix-coated fibre composite consolidation based on a repeating unit cell approach. They have made use of a variational method in which velocity fields for the fibre matrix coating are assumed, and Hill's minimum principle for velocities (Hill, 1956) is used to derive constitutive equations for deformation which minimise the power functional. The model so far has only been developed for square array packing of coated fibres of which the configuration involves less complex

calculation. In general, stacks of coated fibres are likely to fall into hexagonal array configuration as it is the most stable configuration. However, in practical composite component manufacturing processes, the localised regions of reinforcement in components usually contain a combination of square array and hexagonal array packing. The inhomogeneous arrangement could cause by the friction at the interface between the composite and the bulk material as well as deformable die and punch. It is therefore necessary to consider the influences of different fibre packing on consolidation.

This research therefore attempts to develop a new physically based composite consolidation model for hexagonal array packing in order to address the fiber packing issue. Hence, consolidation of composite specimen, which contains a combination of square array and hexagonal array packing, can be simulated.

## 2. Consolidation processes and modelling

Consolidation conditions have significant effects on the mechanical properties of the final composites. It is therefore necessary to carefully choose processing variables and processing setups to obtain optimal conditions for consolidation and that any material damage during consolidation, such as fibre breakage or excessive reactions can be avoided. Thus, ideal conditions for fully dense final composite component with optimum physical and chemical properties can be obtained. Consolidation is determined by three main process variables: temperature, pressure and time. A high temperature enhances the deformation processes which leads to more rapid consolidation. However, it usually leads to excessive interfacial reaction (Guo and Derby, 1994), undesirable grain growth or microstructures (Ward-Close and Loader, 1995) and high levels of residual stresses during cooling from consolidation temperature to room temperature (Guo and Derby, 1995). Although a high consolidation pressure reduces the time and temperature needed for full consolidation of the composite, it usually leads to high local contact pressures which may cause radial fibre damage and cracking or decohesion of the fibre coating. A long consolidation time increases both structural defects and interface reactions. The consolidation time therefore should be kept to a minimum. A compromise has to be found for the heating and pressure components of the consolidation cycles. Modelling of the consolidation process allows predictions of optimum temperature, pressure and time required to obtain fully dense composites with satisfied engineering properties. A number of models has been established for the MCF method

(Wadley et al., 1997; Kunze and Wadley, 1997; Kunze and Wadley, 1998; Elzey et al., 1998; Schuler et al., 2000; Akinsanya et al., 2001; Carmai, 2001; Carmai and Dunne, 2003).

Schuler and co-workers (2000) have developed a micromechanical finite element model for the consolidation of matrix-coated fibres using HIPing. The finite element unit cell consists of the elastic fibre and the matrix which deforms by plastic flow and power-law creep. Akisanya and coworkers (2001) have also developed a micromechanical finite element model for the densification of a square array matrix-coated fibres by rate-independent plastic deformation for both hydrostatic and uniaxial compactions. The plane strain unit cell consists of a quarter of cylinder of which deformation is modelled by two rigid flat punches, indenting the cylinder. Elastic-perfectly plastic and strain-hardening matrix materials are considered. The fibre is assumed to be linear elastic. Their finite element prediction of the evolution of the relative density with pressure response is fairly comparable with experimental results obtained using pseudo-materials consisting of steel cylinders coated with plasticine. The model of Akisanya et al. (2001) has considered only a timeindependent plasticity mechanism. However, the consolidation processes of the MCF composites usually take place at elevated temperature (that is by hot isostatic pressing or vacuum hot pressing) at which the dominant mechanisms are creep and diffusion rather than time independent plasticity. The works of Akisanya (2001) and Schuler (2000) address in particular the development of micromechanical finite element models for consolidation. In other words, finite element meshes are generated to represent explicitly the matrix and fibre in the coated-fibre composite. The work leads to an understanding of the effects of stress, strain and strain rate on the deformation and porosity evolution during consolidation, but cannot provide constitutive equations which are essential for process simulation, as opposed to material simulation. In addition, it is computationally prohibitive to simulate the whole array of coated fibres which are compacted to produce a component. Wadley and co-workers have developed constitutive models for consolidation of matrix-coated fibres. The model development is divided into two stages similar to the development of models for powder consolidation. A large number of parameters are required which need to be predetermined using repetitions of explicit finite element modelling of fibre and matrix material which is computationally intensive. In addition, the model contains arbitrary empirical parameters which have been introduced to account for the different geometries between the initial stage and the final stage.

Carmai and Dunne (2001, 2003) have developed physically based constitutive equations for consolidation of matrix-coated fibre composites based on a repeating unit cell approach. Unit cells

representing square array packing of the coated fibres under symmetric in-plane compressive load have been established and taken into account the power-law creep of the matrix. By consideration of assumed velocity fields in the deforming matrix in terms of an unknown parameter, the dependence of the deformation rate on volume fractions of voids and fibres has been derived through the use of Hill's minimum principle for velocities (Hill, 1956). Hence, the densification rate has been obtained.

# 3. Constitutive model development

A new physically based composite consolidation model for hexagonal array packing has developed by adopting Carmai and Dunne (2003) approach in which in which the constitutive behaviour of a representative volume element (a unit cell) of composite is modelled and then used to predict the macroscopic response.

#### 3.1. Assumptions and basic concepts of the model

For theoretical modelling, it is necessary to make assumptions to simplify calculations. In the present work, matrix-coated fibres are assumed to form a symmetrical, periodic array, repeating in two directions. The coated fibres are assumed to be perfect circular cylinders of infinite length so plane strain conditions hold on planes perpendicular to the fibre axis. The fibre is normally much harder than the matrix. It does not undergo plastic deformation at the temperature of processing. The present analyses consider it to be rigid while the matrix material is incompressible and considered to deform by power-law creep. Uniaxial power-law creep is given by

$$\dot{\varepsilon} = A\sigma^{\,\mathrm{n}} \tag{1}$$

where A is a creep constant and n is the creep exponent. The uniaxial power-law equation can be generalised into multiaxial form

$$\dot{\varepsilon}_{ij} = \frac{3}{2} A \sigma_e^{n-1} S_{ij} \tag{2}$$

 $\sigma_e$  denotes effective stress defined by

$$\sigma_e^2 = \frac{3}{2} S_{ij} S_{ij} \tag{3}$$

where  $S_{ij} = \sigma_{ij} - \delta_{ij}\sigma_m$  is the deviatoric stress and  $\sigma_m$  is the mean stress.

The analyses assume a perfect interface between fibres and matrix and sticking friction at the matrix-matrix interface (that is, no relative, sliding motion between contacting matrix material is allowed). In this work we consider hexagonal array packing of coated fibres subjected to

symmetric in-plane compressive loads, *T*. Due to symmetry, the unit cell considered here is one twelfth of a hexagonal as shown in figure 1.

The approach adopted here is to assume the form of velocity fields developed in the matrix coating during consolidation. A single free parameter is included in the functional forms chosen for the velocity fields. Hill's minimum principle is then invoked at every step of the consolidation in order to determine the value of the free parameter. The velocity fields are therefore continuously evolving during the consolidation in order to satisfy Hill's minimum principle. In the next section, the conditions imposed upon the choice of velocity fields by the requirement of incompressibility of the matrix are explained.

### 3.2. The matrix coated fibre during consolidation

Figure 2 shows schematically the unit cell during consolidation subjected to applied pressure, T. The matrix material is divided into 3 regions for  $\theta$ : region I:  $0 \le \theta \le \gamma$ , region II:  $\gamma < \theta \le \beta$  and region III:  $\beta < \theta \le \frac{\pi}{6}$  in which  $\theta$  is any general angle,  $\gamma$  is an angle obtained from geometry and is given by

$$\gamma = \cos^{-1}(\frac{R - X}{R}) \tag{4}$$

and  $\beta$  is determined to ensure that incompressibility is satisfied. The matrix boundary in regions I and II which is in contact with another coated fibre has the imposed horizontal velocity of  $-\dot{X}$ . A function  $u(\beta,\theta)$ , which describes the profile of the boundary of the matrix in region III, is given by

$$u(\beta,\theta) = R * \sqrt{\cosh(\beta^3(\theta - \beta)) + \sin(\beta^3(\theta - \beta))}$$
 (5)

where

$$R^* = R \frac{\cos \gamma}{\cos \beta} \tag{6}$$

and is shown in figure 2.

The function  $u(\beta, \theta)$  is chosen arbitrarily to ensure that the following boundary conditions are satisfied:

- if  $\beta=0$  then  $u(\beta,\theta)=R$
- if  $\theta = \beta$  then  $u(\beta, \theta) = R^*$
- if  $((\theta = \frac{\pi}{6}))$  and  $(\beta = \frac{\pi}{6})$  then  $u(\beta, \theta) = R^*$

 $\beta$  is determined by imposing the incompressibility condition, i.e. the volume of the matrix material which is lost in region I (VI) is equal to the volume of the matrix material which is gained (V2 +V3) in regions II and III

$$V1 = V2 + V3 \tag{7}.$$

Since plane strain is assumed for the coated fibres, there is no change in length along the fibre direction. Let h be the length of the coated fibre.

V1, the volume of material lost in region I, is given by

$$V1 = \left( \left( \pi R^2 \times \frac{\gamma}{2\pi} \right) - \frac{1}{2} R^2 \sin \gamma \cos \gamma \right) \times h$$

$$= \left( \frac{R^2}{2} (\gamma - \sin \gamma \cos \gamma) \right) \times h$$
(8)

V2, the volume of material gained in region II, is given by

$$V2 = \left(\frac{1}{2}(R * \cos \beta)(R * \sin \beta) - \frac{1}{2}R^{2} \sin \gamma \cos \gamma - \frac{(\beta - \gamma)}{2\pi} \times \pi R^{2}\right) \times h$$

$$= \left(\frac{1}{2}R *^{2} \cos \beta \sin \beta - \frac{1}{2}R^{2} \sin \gamma \cos \gamma - \frac{R^{2}}{2}(\beta - \gamma)\right) \times h$$
(9)

and V3, the volume of material gained in region III, is given by

$$V3 = \int_{\beta}^{\frac{\pi}{6}} \int_{R}^{u(\beta,\theta)} r dr d\theta \times h$$

$$= \frac{1}{2} \int_{\beta}^{\frac{\pi}{6}} ((u(\beta,\theta))^{2} - R^{2}) d\theta \times h$$
(10)

$$V3 = \frac{h^{\frac{\pi}{6}}}{2} \int_{\beta}^{\pi} (u(\beta, \theta))^2 d\theta - \frac{R^2}{2} \left(\frac{\pi}{6} - \beta\right)$$
 (11)

Substituting equations (8), (9) and (11) into (7) gives

$$\frac{R^2}{2}(\gamma - \sin\gamma\cos\gamma) = \frac{R^2}{2}(\cos^2\gamma\tan\beta - \sin\gamma\cos\gamma - \beta + \gamma) + \frac{1}{2}\int_{\beta}^{\frac{\pi}{6}}(u(\beta, \theta))^2d\theta - \frac{R^2}{2}\left(\frac{\pi}{6} - \beta\right)(12)$$

Hence, rearranging

$$\int_{\beta}^{\frac{\pi}{6}} (u(\beta,\theta))^2 d\theta = R^2 \left( \frac{\pi}{6} - \cos^2 \gamma \tan \beta \right)$$
 (13)

 $u(\beta, \theta)$  is given in equation (5) therefore

$$\int_{\beta}^{\frac{\pi}{6}} (u(\beta,\theta))^2 d\theta = \int_{\beta}^{\frac{\pi}{6}} R^{*2} \left( \cosh \beta^3 (\theta - \beta) + \sin \beta^3 (\theta - \beta) \right) d\theta$$

$$= \frac{R^{*2}}{\beta^3} \left( \sinh \beta^3 (\frac{\pi}{6} - \beta) - \cos \beta^3 (\frac{\pi}{6} - \beta) + 1 \right)$$
(14)

Combining (13) and (14) then gives

$$\frac{\cos^2 \gamma}{\cos^2 \beta} \frac{1}{\beta^3} \left( \sinh \beta^3 \left( \frac{\pi}{6} - \beta \right) - \cos \beta^3 \left( \frac{\pi}{6} - \beta \right) + 1 \right) = \left( \frac{\pi}{6} - \cos^2 \gamma \tan \beta \right)$$
 (15)

 $\beta$  is evaluated using a Newton zero-finding routine. Note that  $\beta$  is determined to ensure overall incompressibility of the matrix and this is clearly reflected in the function u, given in equation (5). This, in turn, influences the velocity fields chosen, as shown later. In the next section, Hill's minimum principle is described and the velocity fields assumed in the model are presented.

#### 3.3. Energy method based on Hill's minimum principle

Potential energy methods have been used extensively in developing constitutive models to describe the strain rate behaviour of porous materials (Gurson, 1977; Budiansky et al., 1982; Duva and Hutchinson, 1984; Cocks, 1989). One of the pioneering constitutive models for porous materials, which was developed based on micro-mechanical analysis and using the potential method is Cocks' model (Cocks, 1989) in which a lower bound expression for the potential of a porous creeping material was derived in terms of an assumed deformation rate field. Duva and Crow (1994) also developed a predictive model based on the potential energy method for the consolidation of fibres surrounded by porous matrix material. The deformation rate of the cell is estimated through the use of Hill's minimum principle for velocities (Hill, 1956). Inspired by this modelling approach, it has also been possible to develop constitutive equations for consolidation of matrix coated fibre systems by assuming velocity fields in the deforming matrix, and using a repeating cell approach together with Hill's minimum principle for velocities. The principle states that of all kinematically admissible velocity fields ( $v_i$ ), the actual field minimises the functional

$$F = \int_{V} W \, dV - \int_{S} T_{i} v_{i} dS \tag{16}$$

F denotes the total potential energy rate of the body which consists of the strain rate potential (W) and the potential energy rate due to external pressure ( $T_i$ ). V is the volume of the deformed matrix and S is the outer surface where the pressure  $T_i$  is prescribed.

The strain rate potential for incompressible power-law creeping material is defined as

$$W = \int \sigma_{ij} d\dot{\varepsilon}_{ij} = \frac{n}{n+1} \left(\frac{1}{A}\right)^{\frac{1}{n}} (\dot{\varepsilon}_e)^{\frac{(n+1)}{n}} \tag{17}$$

 $\dot{\varepsilon}_e$  is an effective strain rate which is given by

$$\dot{\varepsilon}_e = \left[\frac{2}{3} \left(\dot{\varepsilon}_{ij} \dot{\varepsilon}_{ij}\right)\right]^{\frac{1}{2}} \tag{18}$$

The usual admissibility means that  $v_i$  satisfies the zero velocity boundary condition at the fibre-matrix interface and the strain rate components are defined as

$$\dot{\varepsilon}_{ij} = \frac{1}{2} (v_{i,j} + v_{j,i}) \tag{19}$$

where , j denotes differentiation with respect to  $x_i$ .

In order to use Hill's minimum principle in the present analysis, a single free parameter,  $\lambda$ , is introduced into the imposed horizontal velocity. For the boundary value problems arising from the cell model as described previously (see section 3.1 and 3.2), velocity fields can be constructed as described below.

Regions I and II are those in which two coated fibres are in contact. The matrix boundary in these regions has horizontal velocity,  $-\lambda \dot{X}$ , imposed upon it. The radial velocity at the matrix boundary is then given by

$$v_{r_{\text{at matrix boundary}}} = -\lambda \dot{X} \cos \theta \tag{20}$$

The radial velocity of the matrix boundary in region III can be obtained by differentiating the function  $u(\beta,\theta)$ . The analysis assumes a nonlinear variation in velocity between fibre surface and the matrix boundary at a typical radial distance, r, for radial velocities in all regions. The radial velocities are assumed to be of the following form

$$v_r = \alpha_3 (\tanh(\alpha_1(r-f))^{\alpha_2}$$
 (21)

 $\alpha_1$  and  $\alpha_2$  are constants of 0.01 and 5 respectively. They are chosen such that the radial velocities are in overall good agreement with those calculated from a finite element model.  $\alpha_3$  is a function of both r and  $\theta$  and is chosen such that the following boundary conditions are satisfied:

For regions I and II  $(0 \le \theta \le \beta)$ :

• if r = f then  $v_r = 0$ ;

• if 
$$r = \frac{R - X}{\cos \theta}$$
 then  $v_r = -\lambda \dot{X} \cos \theta$ .

Hence, an expression for the radial velocity in regions I and II is given by

$$v_{r} = -\frac{\lambda \dot{X} \cos \theta}{\left(\tanh\left(\alpha_{1}\left(r - f\right)\right)\right)^{\alpha_{2}}} \left(\tanh\left(\alpha_{1}\left(r - f\right)\right)\right)^{\alpha_{2}}$$
(22)

For region III  $(\beta < \theta \le \frac{\pi}{6})$ :

- if r = f then  $v_r = 0$ ;
- if  $r = u(\beta, \theta)$  then  $v_r = \dot{u}$ ;

Hence, an expression for the radial velocity in region III is given by

$$v_r = \frac{\dot{u}}{\left(\tanh(\alpha_1(u-f))\right)^{\alpha_2}} \left(\tanh(\alpha_1(r-f))\right)^{\alpha_2}$$
 (23)

The tangential velocity fields are determined by applying plane strain conditions, namely

$$\dot{\varepsilon}_{zz} = 0 \tag{24}$$

Since the matrix material is incompressible,

$$\dot{\varepsilon}_{\theta\theta} = -\dot{\varepsilon}_{rr} \tag{25}$$

From strain rate-velocity relations, equation (25) can be written as

$$\frac{1}{r}\frac{\partial v_{\theta}}{\partial \theta} + \frac{v_r}{r} = -\frac{\partial v_r}{\partial r} \tag{26}$$

Hence, the tangential velocity for region i (i = I, II and III) is given by

$$v_{\theta_i} = \int -\left(r\frac{\partial v_{r_i}}{\partial r} + v_{r_i}\right) d\theta + h(r)$$
(27)

in which h(r) is an arbitrary function of r, and can be determined from boundary conditions. The tangential velocities obtained here satisfy the following boundary conditions.

- if r = f then  $v_{\theta} = 0$ ;
- if  $\theta = 0$  then  $v_{\theta} = 0$ ;
- if  $\theta = \frac{\pi}{6}$  then  $v_{\theta} = 0$ ;
- if  $\theta = \beta$  then  $v_{\theta_{II}} = v_{\theta_{III}}$

An expression for the free parameter  $\lambda$  in terms of applied pressure, the creep parameters, relative density and volume fraction of fibres was determined by applying Hill's minimum principle for velocities. The total potential energy rate for the analysed problem is given by

$$F = \sum_{i=1}^{3} \left( \int_{V_i} W(\dot{\varepsilon}_{e_i}) \ dV_i \right) - \int_{s} T\lambda \dot{X} \ dS$$
 (28)

where  $W(\dot{\varepsilon}_{e_i})$  denotes the strain energy rate in regions *i*. By consideration of relations between strain rate and displacement rate, the effective strain rate,  $\dot{\varepsilon}_e$ , for each region can be obtained.

The functional F is minimised with respect to  $\lambda$ 

$$\frac{\partial F}{\partial \lambda} = 0 \tag{29}$$

giving

$$\lambda = (T\dot{X}(R-X))^{n} \times A \times \left( \int_{0}^{\gamma} \int_{f}^{r} P(\dot{\varepsilon}_{e_{1}}) r dr d\theta + \int_{\gamma}^{\beta} \int_{f}^{r} P(\dot{\varepsilon}_{e_{2}}) r dr d\theta + \int_{\beta}^{\frac{\pi}{4}} \int_{f}^{r} P(\dot{\varepsilon}_{e_{3}}) r dr d\theta \right)^{-n} (30)$$

where

$$P(\dot{\varepsilon}_{e_{i}}) = \frac{n+1}{n} W(\dot{\varepsilon}_{e_{i}}) \frac{1}{\lambda^{\frac{n+1}{n}}}$$
(31).

The relative density, the dilatation rate and the densification rate can be determined as follows. From geometry the relative density, D, which is defined as the ratio of current density to the density at the fully dense state, can be obtained as

$$D = \frac{\left(\frac{m_{fibre} + m_{matrix}}{V_{fibre} + V_{matrix} + V_{void}}\right)}{\left(\frac{m_{fibre} + m_{matrix}}{V_{fibre} + V_{matrix}}\right)} = \frac{V_{fibre} + V_{matrix}}{V_{fibre} + V_{woid}}$$
(32).

So,

$$D = \frac{\frac{1}{12}\pi R^2 L}{\frac{\sqrt{3}}{6}(R - X)^2 L} = \frac{\pi R^2}{2\sqrt{3}(R - X)^2}$$
(33)

The densification rate for the cell can be obtained by differentiating D with respect to time

$$\dot{D} = \frac{\pi \lambda \dot{X}}{R\sqrt{3}\cos^3 \gamma} \tag{34}.$$

Since the overall densification rate is given by

$$\dot{D} = -D\dot{\varepsilon}_{kk} \tag{35}.$$

The overall dilatation rate for the cell is

$$\dot{\varepsilon}_{kk} = \frac{-2\lambda \dot{X}}{R\cos\gamma} \tag{36}$$

Equations (30), (35) and (36) constitute evolution equations for porosity for the fibre-matrix-void system shown in figure 1. Whilst it has not been possible to use the bounding method here to obtain analytical forms for the equations (equation (30), of course, requires numerical integration). Nonetheless, they may be considered to be constitutive equations for fibre-matrix-void systems. This is important because they are of appropriate form for implementation into finite element software, enabling the calculation of the evolution of porosity at each Gauss point in the finite element mesh. The predictive capability of the model is tested by carrying out direct comparisons of predictions made by an equivalent, micro-mechanical finite element model. The finite element model is discussed in the next section.

## 4. Explicit micromechanical finite element model for a symmetric unit cell

An explicit micromechanical finite element model has been developed for hexagonal array packing using ABAQUS which is shown schematically in figure 3. Since the fibre is assumed to be rigid, the finite element mesh is developed only for the matrix which consists of two dimensional plane strain, 4-noded elements. All nodes lying on the fibre-matrix boundary are fixed in both the *x* and *y* directions and those on the lower unit-cell boundary are allowed to move in the *x* direction only while all nodes lying on the upper unit-cell boundary are constrained to remain on the boundary but are free to move along it. A movable boundary is used for the application of the distributed load, simulating the hydrostatic pressure state during the hot isostatic pressing process. The movement of this boundary is restricted to be along the x-axis. Sticking friction is assumed between matrix-matrix interfaces. The matrix is assumed to show power-law creep behaviour. The multiaxial power-law creep equation which is given in equation (2) was implemented into ABAQUS using a UMAT subroutine. Figure 4 shows typical finite element mesh deformation during the consolidation. The deformed profile is similar to the deformed unit cell of the energy method in figure 2. The finite element deformed mesh can also be divided into three regions which are the same as those of the unit cell of the energy method.

#### 5. Process simulation

The model based on the energy method was implemented using standard Fortran 90. A Newton zero-finding routine was used to solve equation (15) to obtain  $\beta$ . A subroutine for evaluating

multiple integrals using the trapezoidal rule (Gerald, 1980) was developed to calculate the value of  $\lambda$ . The initial relative density was taken as 0.9069 for hexagonal packing. For the finite element modelling, the displacement (X) of the movable boundary was recorded with time. This displacement, X, was used to calculate the relative density using equation (33).

A number of analyses of densification behaviour of the Ti-6Al-4V coated-fibre consolidated by HIP have been carried out. The first set was to investigate the influence of applied pressure on the densification. The models based on the energy method, and the micro-mechanical finite element method were set up to simulate the consolidation processes for four different constant applied pressures of 15, 30, 50 and 70 MPa with the same fibre volume fraction of 25% and at a constant temperature of  $900^{\circ}$ C. Material parameters required for the simulations are 1.7 for a creep exponent n and  $1.25 \times 10^{-5}$  for a creep constant (Warren et al., 1995).

The second analysis was carried out to investigate the influence of volume fraction of fibres on the rate of densification. The simulations were conducted using the model based on the energy method and the micro-mechanical finite element model for various volume fractions of fibres at a constant temperature of 900°C and with a constant pressure of 30 MPa. The results of the analyses are presented in the next section.

# 6. Theoretical predictions and comparisons with FEM calculations

#### 6.1. Influence of applied pressure on densification

Figures 5(a) and 5(b) show comparisons of density evolution over time for applied pressures of 15, 30, 50 and 70 MPa obtained from the energy method and the finite element model respectively. The relative density increases very rapidly at relatively low densities and increases slowly at high densities. This is due to low matrix creep rate at high density. It can be seen that the principal part of the composite consolidation occurs within the initial stage, whereas the final stage has only a minimal influence on the composite densification. The predictions from both models show that increasing applied pressure causes reduction in the time at which full density is reached. It can be seen that increasing the applied pressure leads to higher densification rate. Figure 6 shows direct comparison of the relative density evolution over time curves predicted by the energy method and the explicit micromechanical finite element model. The relative density evolution over time curves predicted by the

finite element model for the initial stage of consolidation. At relatively high densities a few differences can be seen

#### 6.2 Influence of volume fraction of fibres on the densification

Figures 7(a) shows the density evolution over time curves for fibre volume fractions of 10%, 25% and 40% obtained from the energy method. It can be seen that as volume fraction of fibres increases, so the time at which the fully dense stage is reached increases, i.e. the densification rate decreases. The higher the volume fraction of fibres the lower the densification rate. This conclusion is supported by simulation results in Duva and Crow (1994); Kunze (1996); Elzey et al. (1998); Kunze and Wadley (1998) and the experimental evidence in Besson and Evans (1992).

Figures 7(b) and 7(c) show comparisons of relative density evolution over time curves predicted by the energy method and the finite element model for 10% and 40% volume fraction of fibres respectively. Reasonably good agreement can be seen for both volume fractions.

# 7. Multiaxial generalisation of the constitutive equations and their finite element implementation

Constitutive equations for consolidation of matrix-coated fibre system developed previously give good representation of the densification behaviour of Ti-6Al-4V coated fibres under symmetric pressures. It is necessary to develop further a multiaxial generalisation of the constitutive equations to make them suitable for general, asymmetric loadings.

A number of multiaxial constitutive models for the consolidation of metal powders (that is, for monolithic materials, and not continuous fibre composites) have been developed over the years. They have been used to predict the dependence of densification rate on consolidation pressure and temperature as well as volume fraction of voids. The pioneering constitutive model for consolidation of metal powder was developed by Wilkinson and Ashby (1975). They analysed the creep collapse of a thick-walled spherical shell subjected to externally applied hydrostatic loading. In general, consolidation occurs under a range of stress states that are not purely hydrostatic. Subsequent research has therefore broadened the Wilkinson and Ashby model to more general loading conditions. The models have taken into account the effect of multiaxial stress state by using potential methods which can make possible the development of relationships between macroscopic strain rate and macroscopic stress state (Cocks, 1989; Ponte Castaneda, 1991;

Sofronis and McMeeking, 1992; Duva and Crow, 1992). The model of Duva and Crow, for example, takes the form

$$\dot{\varepsilon}_{ij} = \frac{\partial \phi}{\partial \sigma_{ij}} = AS^{n-1} \left( \frac{3}{2} a \sigma'_{ij} + \frac{1}{3} b \delta_{ij} \sigma_m \right) \tag{37}$$

where

$$S^2 = a\sigma_e^2 + b\sigma_m^2 \tag{38}$$

$$\sigma_e^2 = \frac{3}{2}\sigma'_{ij}\sigma'_{ij} \tag{39}$$

$$\sigma_{ij}' = \sigma_{ij} - \delta_{ij}\sigma_{m} \tag{40}$$

$$\sigma_m = \frac{1}{3}\sigma_{kk} \tag{41}$$

S is an *effective* effective stress (Duva and Crow, 1992; Duva and Crow 1994) for the porous creeping material. The coefficients a and b are functions of current relative density, D, which is equivalent to the solid volume fraction of the porous material, and the creep exponent, n. a is associated with the equivalent stress term while b is associated with the hydrostatic stress. The various densification models for monolithic materials in the literature use different approaches to obtain the strain rate potential for the porous creeping materials. This leads to different expressions for the coefficients a and b (Duva and Crow, 1992).

The coefficients a and b are chosen such that, at the fully dense state, i.e. D =1, the coefficient b becomes zero and a becomes 1. For this case, the *effective* effective stress, S, is reduced to  $\sigma_e$ .

The densification rate can be obtained from

$$\dot{D} = -D\dot{\varepsilon}_{kk} \tag{42}$$

$$\dot{\varepsilon}_{kk} = \dot{\varepsilon}_{11} + \dot{\varepsilon}_{22} + \dot{\varepsilon}_{33} \tag{43}$$

where D is the relative density and  $\dot{\varepsilon}_{kk}$  is the dilatation rate. By adopting the existing models for consolidation of metal powder, the constitutive equations for the consolidation of matrix-coated fibre composites, presented above, can be generalised into multiaxial form. This is presented in the next section.

#### 7.1 Multiaxial constitutive equations for composite consolidation

The rate of plastic deformation needs to be defined to describe the deformation behaviour of the matrix coated fibre composites. The rate of plastic deformation of a compressible material can be decomposed into two parts as follows:

$$\underline{\mathbf{D}}^{P} = \underline{\mathbf{D}}^{cr} + \frac{1}{3}\dot{\boldsymbol{\varepsilon}}^{sw}\underline{\mathbf{I}}$$
(44)

 $\underline{\mathbf{D}}^{cr}$  corresponds to an incompressible creep term while  $\dot{\mathcal{E}}^{sw}$  corresponds to a swelling term. Equation (37) for monolithic porous materials can be decomposed into two parts which are rewritten in tensor form as

$$\underline{\mathbf{p}}^{P} = \left(\frac{3}{2}AS^{n-1}a\underline{\mathbf{\sigma}}'\right) + \left(\frac{1}{3}AS^{n-1}b\sigma_{m}\right)\underline{\mathbf{I}}$$
(45)

The first term on the right hand side corresponds to conventional creep deformation in a homogeneous material, but in the presence of voids (and as the volume fraction of voids approaches zero, so a approaches unity, and the *effective* effective stress, S, reduces to just the equivalent stress in an incompressible material,  $\sigma_e$ . The first term therefore becomes just conventional, incompressible creep). The second term is the swelling term for a monolithic, homogeneous material containing voids. But in the present work, the swelling strain is just the dilatation rate presented in equation (36) for the matrix-fibre-void system. Hence, for the composite material considered here, the total plastic deformation rate is given by

$$\underline{\mathbf{p}}^{P} = \left(\frac{3}{2} A S^{n-1} a \underline{\mathbf{\sigma}}'\right) + \frac{1}{3} (\dot{\varepsilon}_{kk}) \underline{\mathbf{I}}$$
(18)

where  $\dot{\varepsilon}_{kk}$  is given in equation (36) and the coefficient a is the same as that in Cocks, 1989; Ponte Castaneda, 1991; and Duva and Crow, 1992, i.e.

$$a = \frac{1 + \frac{2}{3}(1 - D)}{D^{\frac{2n}{n+1}}} \tag{19}.$$

The evolution of relative density of the matrix coated fibre composite is described by equations (30), (35) and (37). In order to determine  $\lambda$  (and hence  $\dot{\varepsilon}_{kk}$ ), the pressure T imposed on the repeating cell, as shown in figure 1, is required. In general, the repeating cells will not be subjected to purely hydrostatic stress states. However, it was shown in Carmai (2001) that the densification rate is dominated by the hydrostatic stress, and independent of the equivalent stress. Hence, the pressure T is calculated from

$$T = \sigma_m = \frac{1}{3} \left( \sigma_1 + \sigma_2 + \sigma_3 \right) \tag{48}$$

where  $\sigma_1$ ,  $\sigma_2$  and  $\sigma_3$  are principal stresses.

The displacement X at the end of each time step is determined using the first order Euler's integration scheme

$$X^{t+\delta t} = X^t + (-\lambda \dot{X})\delta t \tag{49}$$

The implementation of the multiaxial model into finite element software is described in the next section.

#### 7.2 Finite element implementation of the multiaxial constitutive equations

The multiaxial constitutive equations have been implemented into the finite element software ABAQUS within a large deformation formulation using a UMAT subroutine. Large deformation theory is necessary, since the strains and rigid body rotation in practical processes can be large ABAQUS supplies to the UMAT subroutine the deformation gradient at the beginning and the end of each time step,  $\underline{\mathbf{F}}^t$ , and  $\underline{\mathbf{F}}^{t+\delta t}$ . The user is required to supply the Cauchy stress at the end of the time step. The algorithms, firstly, need to define the rate of deformation gradient,  $\underline{\dot{\mathbf{F}}}$  which can be calculated, for small time steps, as

$$\underline{\dot{\mathbf{F}}} = \frac{1}{\delta t} (\mathbf{F}^{t+\delta t} - \mathbf{F}^{t}) \tag{49}.$$

Then, the velocity gradient,  $\underline{L}$ , is

$$\underline{\mathbf{L}} = \dot{\underline{\mathbf{F}}} \ \underline{\mathbf{F}}^{-1} \tag{50}$$

The total rate of deformation,  $\underline{\mathbf{D}}$ , and the spin tensor,  $\underline{\mathbf{W}}$ , are given by

$$\underline{\mathbf{D}} = \frac{1}{2} (\underline{\mathbf{L}} + \underline{\mathbf{L}}^{\mathrm{T}}) \tag{51}$$

$$\underline{\mathbf{W}} = \frac{1}{2} (\underline{\mathbf{L}} - \underline{\mathbf{L}}^{\mathrm{T}}) \tag{52}$$

The strain components are calculated independently from

$$\underline{\varepsilon} = -\frac{1}{2} \ln \left( \underline{\mathbf{F}} \underline{\mathbf{F}}^{\mathrm{T}} \right)^{-1} \tag{53}$$

The dilatation rate,  $\dot{\mathcal{E}}_{kk}$ , and the densification rate,  $\dot{D}$ , can be calculated from equations (36) and (35) respectively. The relative density at the end of each time step is determined using the first order Euler integration scheme

$$D^{t+\delta t} = D^t + \dot{D}\delta t \tag{54}$$

The co-rotational stress rate  $\sigma$  is given by

$$\frac{\nabla}{\underline{\sigma}} = \frac{E}{(1+\nu)} \underline{\mathbf{D}}^{e} + \frac{E\nu}{(1+\nu)(1-2\nu)} \operatorname{tr}(\underline{\mathbf{D}}^{e}) \underline{\mathbf{I}}$$
 (55)

where E is Young's modulus, v is Poisson's ratio and  $\underline{\mathbf{D}}^{e}$  is the rate of elastic deformation

$$\mathbf{D}^{\mathbf{e}} = \mathbf{D} - \mathbf{D}^{\mathbf{p}} \tag{56}$$

 $\underline{\mathbf{p}}^{p}$  is the rate of plastic deformation as given in equation (46). The stress rate,  $\dot{\underline{\sigma}}$ , is calculated as

$$\underline{\dot{\sigma}} = \underline{\sigma} + \underline{\mathbf{W}} \cdot \underline{\sigma} - \underline{\sigma} \cdot \underline{\mathbf{W}}$$
 (57)

Finally, the stress,  $\underline{\sigma}$ , for each time increment can be determined by utilising the first order Euler integration scheme

$$\underline{\sigma}^{t+\delta t} = \underline{\sigma}^t + \underline{\dot{\sigma}}\delta t \tag{58}$$

The validity of the multiaxial generalisation of the constitutive equations is assessed by comparing the results obtained with those obtained from explicit micromechanical finite element calculations.

# 8. Explicit micromechanical finite element model for asymmetric pressure application

The explicit micromechanical finite element model developed in section 2.4 has been modified for asymmetric pressure application. The unit cell must be one sixth of a hexagonal. The model is shown schematically in figure 8. The coated fibres are assumed to be perfect cylinders of infinite length so plane strain conditions hold on planes perpendicular to the fibres axis. The matrix is assumed to obey power-law creep behaviour while the fibre is assumed to be rigid. All nodes lying on the fibre-matrix boundary are fixed in both the *x* and *y* directions and those on the lower unit-cell boundary are allowed to move in the *x* direction only while all nodes lying on the upper unit-cell boundary are constrained to remain on the boundary but are free to move along it.

Two movable boundaries are used for the application of the distributed load, simulating the pressure state during the consolidation process. They are tangent to the matrix coatings. The

movement of the right movable boundary is restricted to be along the x-axis. The other movable boundary must remain perpendicular to the upper unit cell boundary during the consolidation. Sticking friction is assumed between matrix-matrix interfaces.

# 9. Comparisons with explicit micromehenaical finite element calculations

The first analysis of densification behaviour of the Ti-6Al-4V coated fibres has been carried out for a symmetric pressure application in order to validate the implementation of the generalised mutiaxial constitutive equations into ABAQUS. The predictions obtained from the multiaxial constitutive model have been compared with those obtained from an independent numerical implementation of the constitutive equations for symmetric loads using Fortran, and the explicit micromechanical finite element model. The consolidation behaviour of matrix-coated fibre composites has been simulated by imposing constant, symmetric pressures of 50 MPa onto a single plane strain element in both the x and the y directions. The consolidation temperature is 900°C with a volume fraction of fibres of 25%. The coated fibres are assumed to be perfectly circular and uniformly distributed within the element. Figure 9 shows comparisons of relative density evolution with time curves obtained from the multiaxial constitutive model, the explicit micromechanical finite element model, and the numerical implementation of the constitutive equations for symmetric loading. The prediction obtained from the multiaxial constitutive model shows good agreement with that obtained from the independent numerical implementation. Differences can be seen at relatively high density when compared with the prediction obtained from the explicit micromechanical finite element model. The total consolidation time predicted by the multiaxial constitutive model is less than that predicted by the explicit micromechanical finite element model.

The second set of analyses have been carried out for asymmetric pressure application for pressure couple 30/70 MPa and 20/40 MPa with fibre volume fraction of 25% and at a constant temperature of 900°C. The coated fibres are assumed to be perfectly circular and uniformly distributed within the element. Figure 10 shows comparisons of relative density evolution with time obtained from the finite element multiaxial constitutive model and the explicit micromechanical finite element model for pressure couple 30/70 MPa and 20/40 MPa. The results show good agreement and therefore lend confidence in the generalisation of the model for complex stress states.

# 10. Model validation with experiments

#### 10.1 Model simulations

The ability of the model to predict the real densification bahaviour has been tested using the results of the experiments of Peng et al. (2005). Peng et al (2005) conducted experiments to investigate the consolidation behaviour of Ti-6Al-4V matrix-coated SiC fibres under uniaxial constrained compression loading. Pre-coated fibres of 245 µm diameter have been bounded to form a layer. Six layers of bounded coated fibres were then positioned within a nickel-based superalloyed channel die to form a composite material specimen with hexagonal array packing. The number of fibre was alternated layer by layer with a difference of one fibre in each layer, that is ,with fibre numbers of 24/2324/23...24/23. Hence, the overall size of fibre-ply is 5.88 mm width and 1.306 mm height and has 35% volumn fraction of fibres. The lay-up of fibres were then consolidated by uniaxial, vacuum hot pressing. A constant load of 30 MPa was applied to the fibre-ply when the consolidation temperature of 900°C was reached. The current height of the specimen has been obtained directly from an extensometer

A finite element model was set up, as shown schematically in figure 11, to simulate the experiment. The fibre-ply specimen was modelled using a single plane strain element. The movement of left and right boundaries of the model were constrained in the horizontal direction. The bottom boundary of the model was constrained in the vertical direction. The top boundary of the model was subjected to a vertical compressive load. The multiaxial constitutive equations presented above require the creep properties of the matrix coating to be known over the appropriate range of temperature. The creep parameter A and exponent n for the matrix material at  $900^{\circ}$ C were obtained from the a single fibre test conducted by Peng et. al. (2005). They are  $1.23 \times 10^{-5}$  and 1.3 respectively. Volume fraction of fibres and the initial relative density are also required for model simulations. The volume fraction of fibres was set to be 35% and the initial relative density was set to 0.906, assuming hexagonal array packing.

### 10.2 Comparisons of predicted and experimental results

Figure 12 shows a comparison of predicted and experimental overall vertical displacement versus time curves. It can be seen that the vertical displacement slightly overestimates the experimental measures. However, in overall, reasonably good agreement can be achieved. Figure 13 shows comparisons of predicted and experimental relative density versus time curves. The model simulation tends to underestimate slightly the total consolidation time. The differences may be explained in several ways. The model assumes cusped voids throughout the consolidation process but, in practice, when a composite approaches the fully dense state, the void shape tends to become spherical which results in slower densification rates at near full consolidation (Liu et. al., 1994; Qian et. al.,1996). In addition, the heating of the sample in practice may not be perfectly homogeneous resulting in small variations in temperature within the deforming specimen. Furthermore, despite the use of a diffusion bonding inhibitor, it is never possible to eliminate frictional effects between specimen and die.

The matrix-coated fibre consolidation model for square array packing which was developed in ( Carmai and Dunne, 2004), have been employed to simulate the same experiment. The predicted results obtained from the square array packing simulation and from the hexagonal array packing simulation have been compared with the experimental result of Peng et. al (2005). This experiment represents a practical case of component manufacture where the fibre rearrangement occurs due to the die deformation at high temperature and hence less constraint imposed on the fibre side way motion (Peng et al., 2003). In addition, in practical composite component manufacturing processes, the localised regions of reinforcement in components usually contain a combination of square array and hexagonal array packing. A comparison of the normalized displacement versus time curves obtained from the two simulations and the experiment is shown in figure 14. The ram displacement was normalised by the measured total displacement for each particular fibre array. When comparing the results obtained from the simulations with square array packing and with the hexagonal packing, it is seen that the time required to achieve fully dense material was shorter for the hexagonal packing, and the displacement required to achieve this was smaller. This is obvious because the initial relative density of hexagonal array configuration is higher than that of square array configuration. It can be seen in figure 14 that the normalised displacement curve versus time obtained from the experiment is bounded by the two predicted curves. The typical dynamic densification curves for consolidating both hexagonal array and square array fibre packing under uniaxial hot pressing are given in figure 15. The densification curves for hexagonal array and square array fibre packing provide the upper and lower bounds,

respectively. It is suggested that, for a practical process where fibre re-arrangement occur, the densification curve falls between the 2 curves, for example as indicated by the square symbol in figure 15.

# 11. Concluding Remarks

Physically based constitutive equations for consolidation of matrix-coated fibre composites which are arranged in hexagonal array configuration were developed using the micromechanical modelling. The model was firstly developed for symmetric in-plane compressive load and based on a variational method in which assumed velocity fields in the deforming matrix were considered and were expressed in terms of an unknown parameter. In this way, the dependence of the deformation rate on volume fraction of voids and fibres was derived through the use of Hill's minimum principle for velocities. Explicit micromechanical finite element models in which fibre, matrix and void are modelled explicitly were also developed for validation and comparison. Theoretical predictions were examined. The constitutive equation for consolidation derived from Hill's minimum principle shows good agreement with results obtained from micromechanical finite element modelling.

The resulting constitutive equations was subsequently generalised to multiaxial stress states. The total deformation of the consolidating composite was expressed as the sum of a conventional deviatoric creep term, together with a dilatational term, which was described by the derived constitutive equations. The multiaxial constitutive equations were implemented into finite element software at the continuum level within a finite deformation framework to enable simulations of practical manufacturing processes. The model predictions show good agreement with the predictions obtained from micromechanical finite element simulations. The analyses show that high applied pressures enhance densification rate. Furthermore, increasing the volume fraction of fibres leads to a reduction in densification rate. The resulting constitutive model has been employed to simulate an experiment. Creep data for the Ti-6Al-4V matrix coating obtained from Peng et al (2005) were used. Good agreement between the results has been achieved. The model predictions indicate that a longer consolidation time is required for densifying square fibre arrays than that for a hexagonal array under the same conditions of temperature and pressure. It

can be drawn from comparisons of predicted and experimental results that for practical consolidation process where a combination of square array and hexagonal array packing of fibre appears, the densification curve falls between the densification curves obtained from pure hexagonal array packing and pure square array packing.

#### 12. References

Akisanya, A.R., Zhang, Y., Chandler, H.W., Henderson, R.J., 2001. The deformation and densification of an array of metal-coated fibres. Acta Materialia 49, 221-235.

Budiansky, B., Hutchison, J.W., Slutsky, S., 1982. void growth and collapse in viscos solids. In: Hopkins, H.G., Sewell, M.J., (Eds.), Mechanics of Solids, The Rodney Hill 60th Anniverary Volume. pp. 13-45.

Cocks, A.C.F., 1989. Inelastic deformation of porous materials. Journal of the Mechanics and Physics of Solids 37(6), 693-715.

Carmai, J., 2001, The modelling of matrix-coated fibre composite consolidation. D.Phil Thesis, University of Oxford.

Carmai, J., Dunne, F.P.E., 2003, Constitutive equations for densification of matrix-coated fibre composite during hot isostatic pressing. International Journal of Plasticity, 19(3), pp. 345-363.

Carmai, J., Dunne, F.P.E., 2004, Generalised constitutive equations for densification of metal matrix coated fibre composites. Material science and technology, 20, 478-484.

Duva, J.M., Hutchinson, J.W., 1984. Constitutive potentials for dilutely nonlinear materials. Mechanics of Materials, 3, 41-54.

Duva, J.M., Crow, P. D. 1992. The Densification of Powders by Power-Law Creep During Hot Isostatic Pressing. Acta Metallurgica et Materialia 40(1), 31-35.

Duva, J.M., Crow, P.D., 1994. Analysis of consolidation of reinforced materials by power-law creep. Mechanics of Materials 17, 25-32.

Elzey, D.M., Gampala, R., Wadley, H.N.G., 1998. Inelastic contact deformation of metal-coated fibers. Acta Materialia 46(1), 193-205.

Gerald, C.F., 1980. Applied Numerical Analysis. Addison-Wesley.

Guo, Z.X., Derby, B. 1994. Theoretical model for solid-state consolidation of long-fibre reinforced metal-matrix composites. Acta Metallurgica et Materialia 42 (2), 461-473.

Guo, Z.X., Derby, B., 1995. Solid state fabrication and interfaces of fibre-reinforced metal matrix composites. Progress in Material science 39, 411.

Gurson, A.L., 1977. Continuum theory of ductile rupture by void nucleation and growth: Part 1 - Yield criteria and flow rules for porous ductile media. Journal of Engineering Materials and Technology 99(1), 2-15.

Hill, R., 1956. New horizons in the mechanics of solids. Journal of the Mechanics and Physics of Solids 5, 66-74.

Kunze, J.M., Wadley, H.N.G., 1997. The densification of metal coated fibers: hot isostatic pressing experiments. Acta Materialia 45(5),1851-1865.

Kunze, J.M., Wadley, H.N.G., 1998. The vacuum hot pressing behavior of silicon carbide fibers coated with nanocrystalline Ti-6Al-4V. Materials Science and Engineering A, 138-144.

Peng H.X., Dunne F.P.E., Baik, K.H., Grant, P.S., 2003. Fibre re-arrangement and matrix softening phenomena in matrix-coated fibre (MCF) composite during vacuum hot pressing. Materials Science and Engineering A, 246-253.

Peng H.X., Dunne F.P.E., Grant, P.S., Cantor, B. 2005. Dynamic densification of matrix-coated composite modeling and processing. Acta Materialia, (in press).

Ponte Castaneda, P., 1991. The Effective Mechanical Properties of Nonlinear Isotripic Composites. Journal of the Mechanics and Physics of Solids 39(1), 45-71.

Sofronis, P., McMeeking, R.M., 1992. Creep of Power-Law Material Containg Spherical Voids. J. App.Mech., Trans ASME 59(2), 88-95.

Schuler, S., Derby, B., Wood, M., WardClose, C.M., 2000. Matrix flow and densification during the consolidation of matrix-coated fibres. Acta Materialia 48, 1247-1258.

Wadley, H.N.G., Davison, T.S., Kunze, J.M., 1997. Densification of metal coated fibers by elastic-plastic contact deformation. Composites Part B 28B, 233-242.

Ward-Close, C.M., Loader, 1995. PVD precessing of fibre reinforced composites. In: Froes, F.H., Storer, J. (Eds.), Recent advances in Ti-metal matrix composites, Materials week, TMS Fall, pp. 19-32.

Warren, J., Hsiung, L.M., Wadley, H.N.G., 1995. High temperature deformation behaviour of physical vapour deposited Ti-6Al-4V. Acta Metallurgica et Materialia 43(7), 2773-2787.

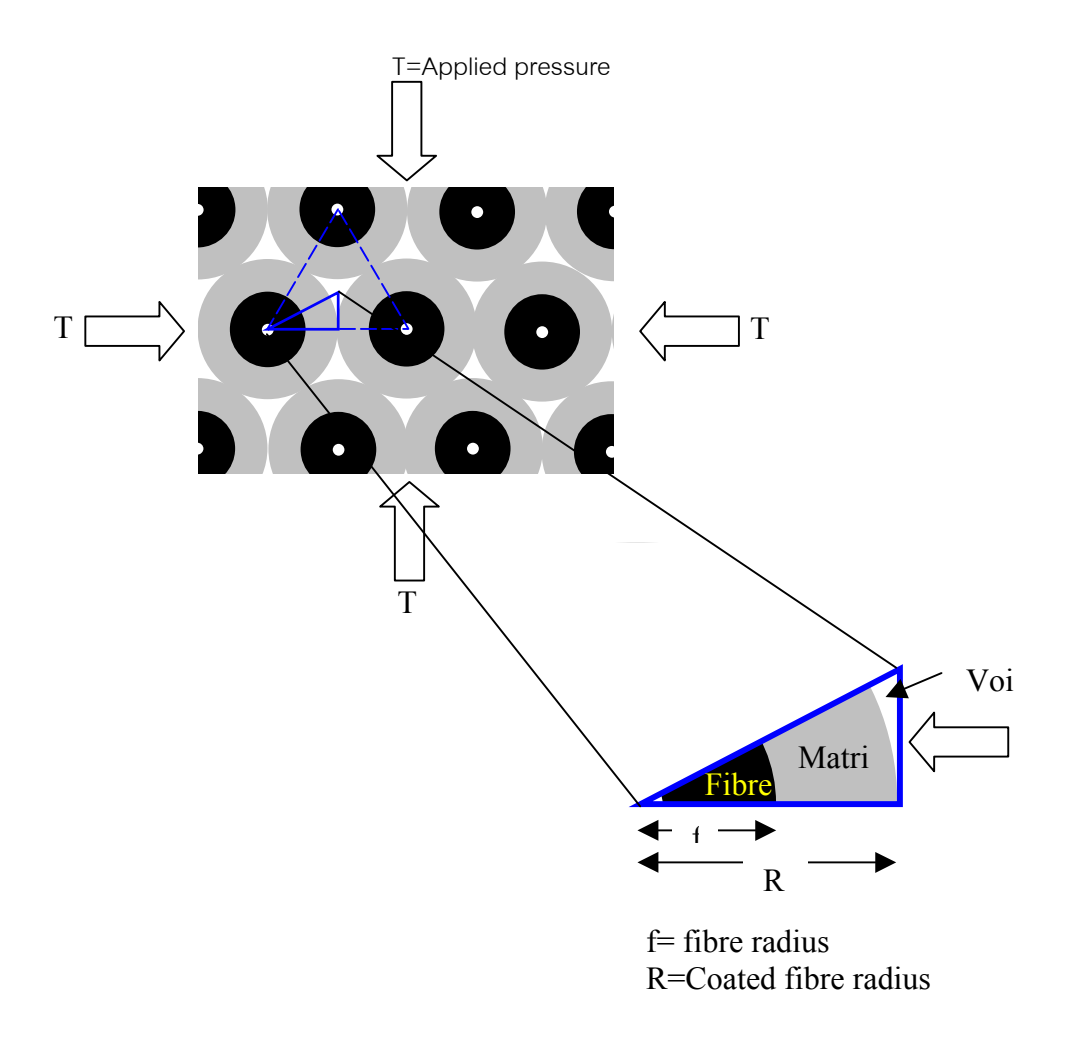


Figure 1 Unit cell representation for hexagonal array packing of coated fibres

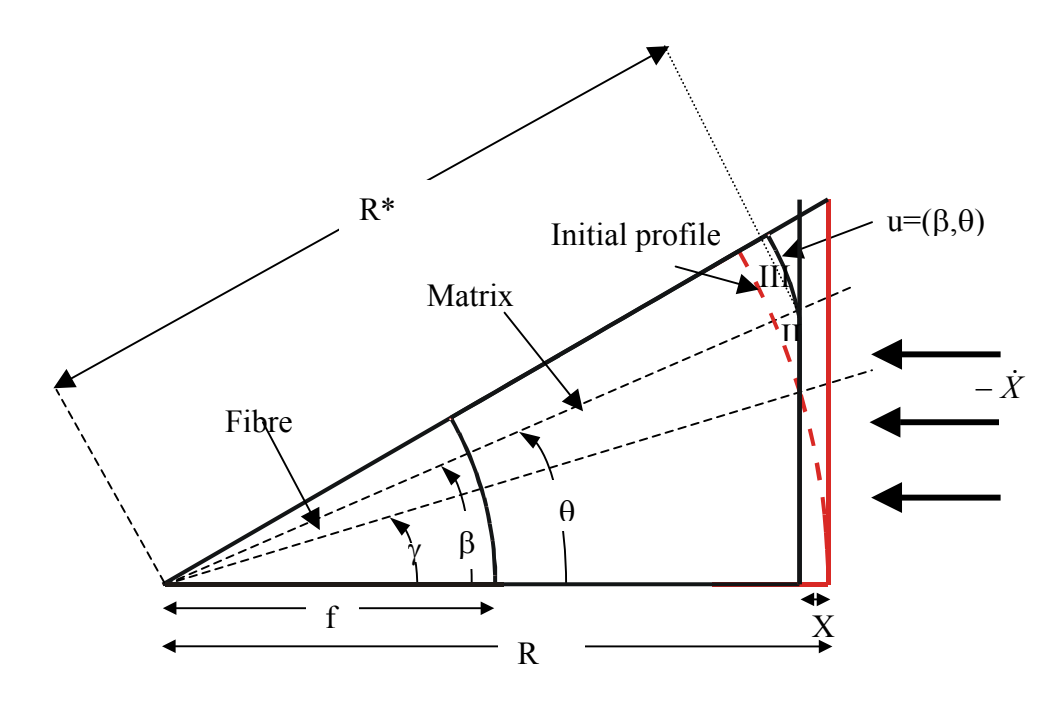


Figure 2 Schematic diagram showing the unit cell during consolidation.

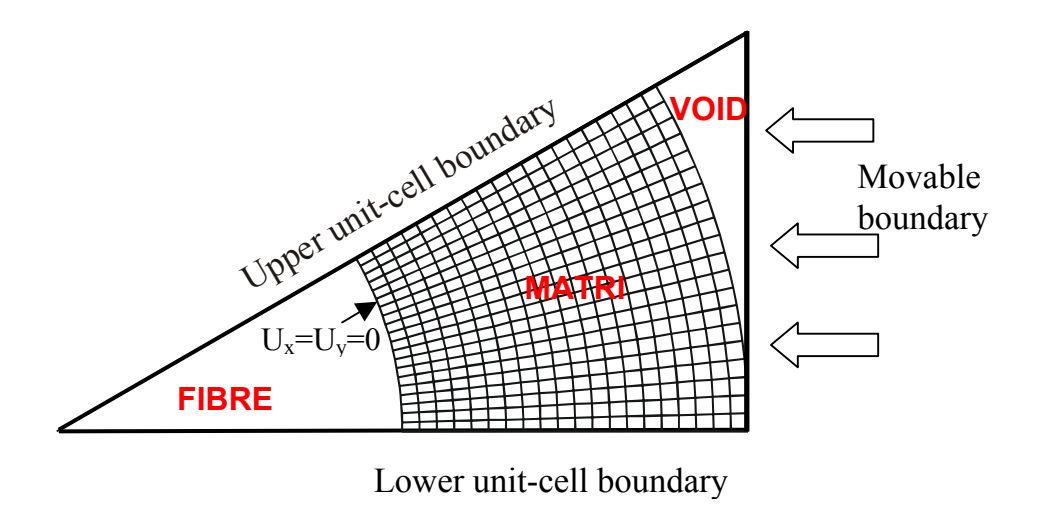


Figure 3 Schematic diagram showing the micromechanical finite element model.

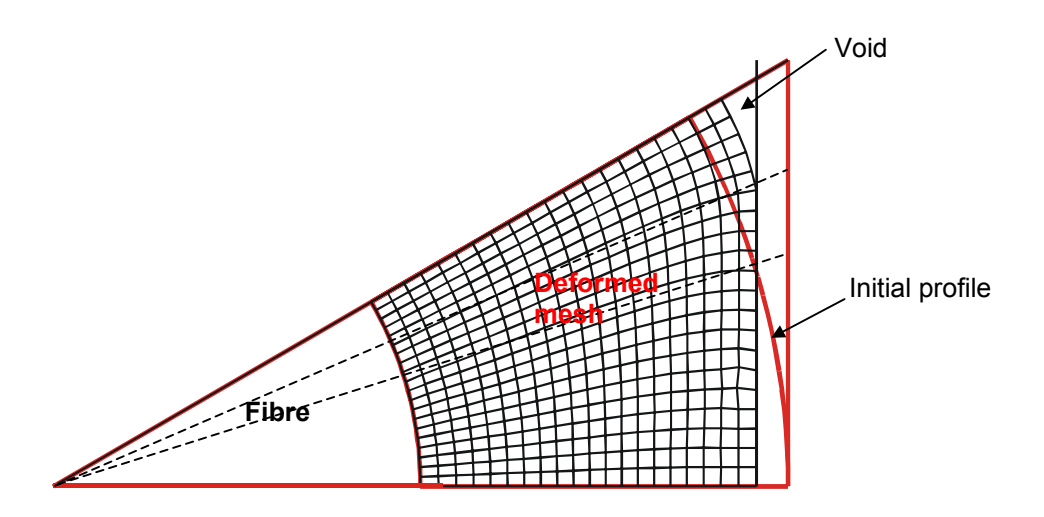


Figure 4 Finite element mesh deformation during consolidation.

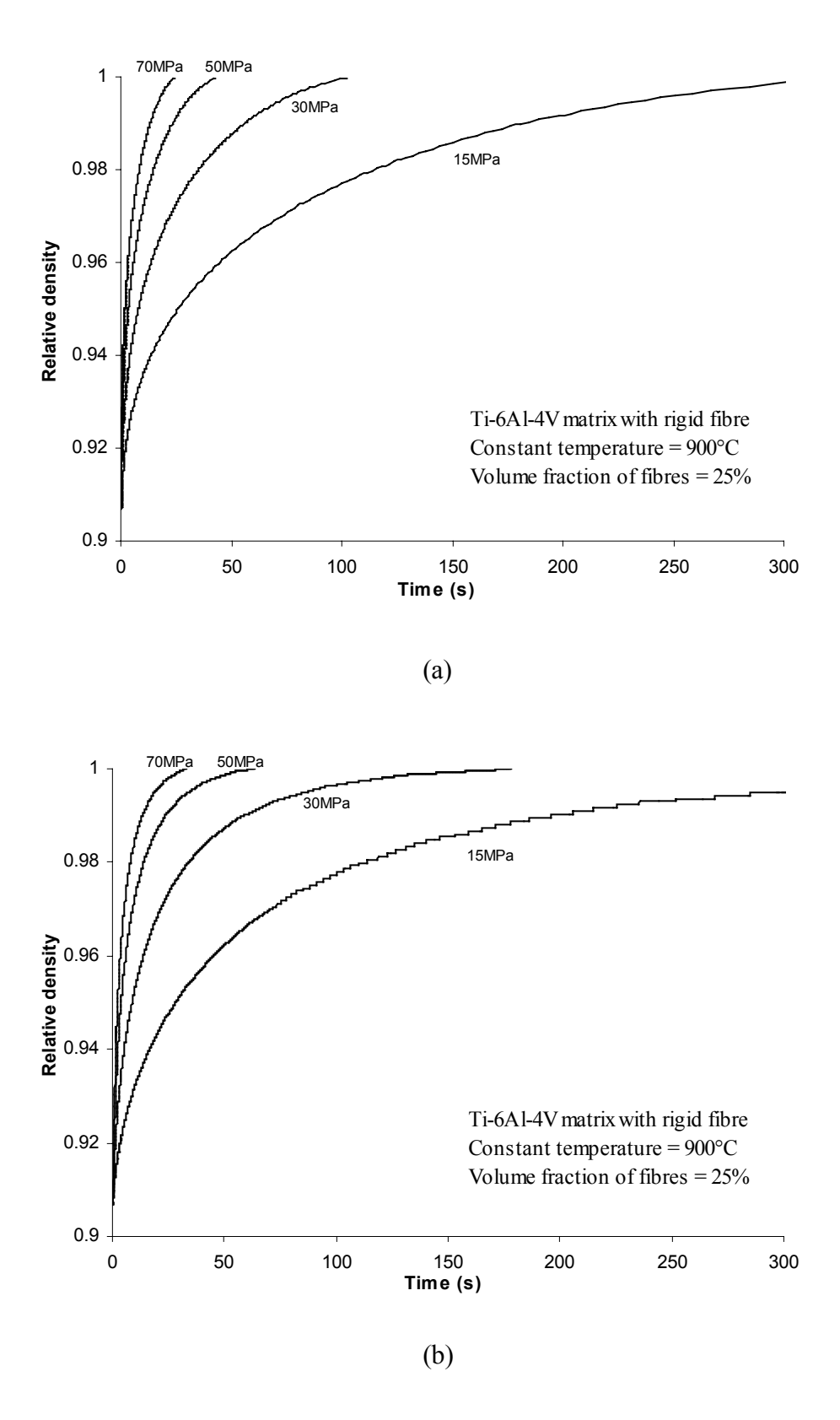
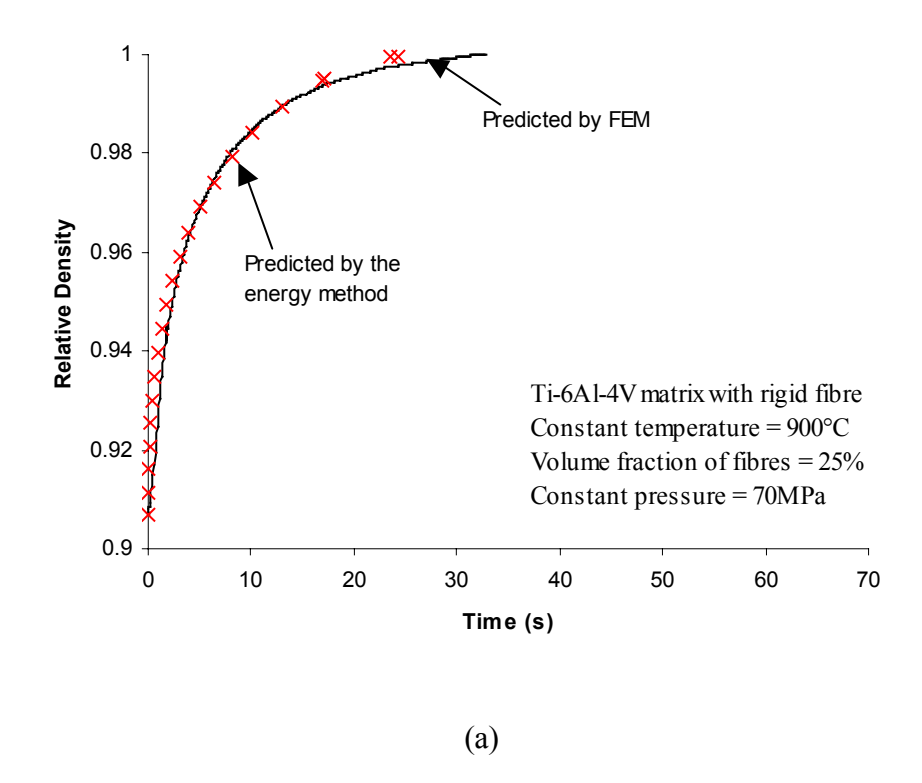
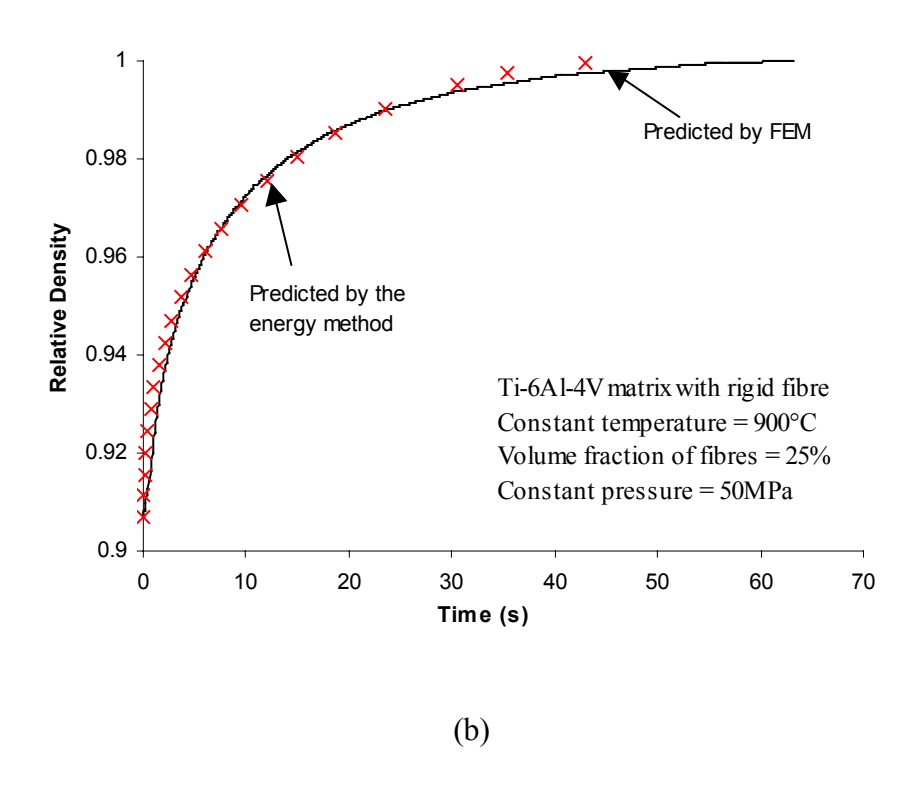
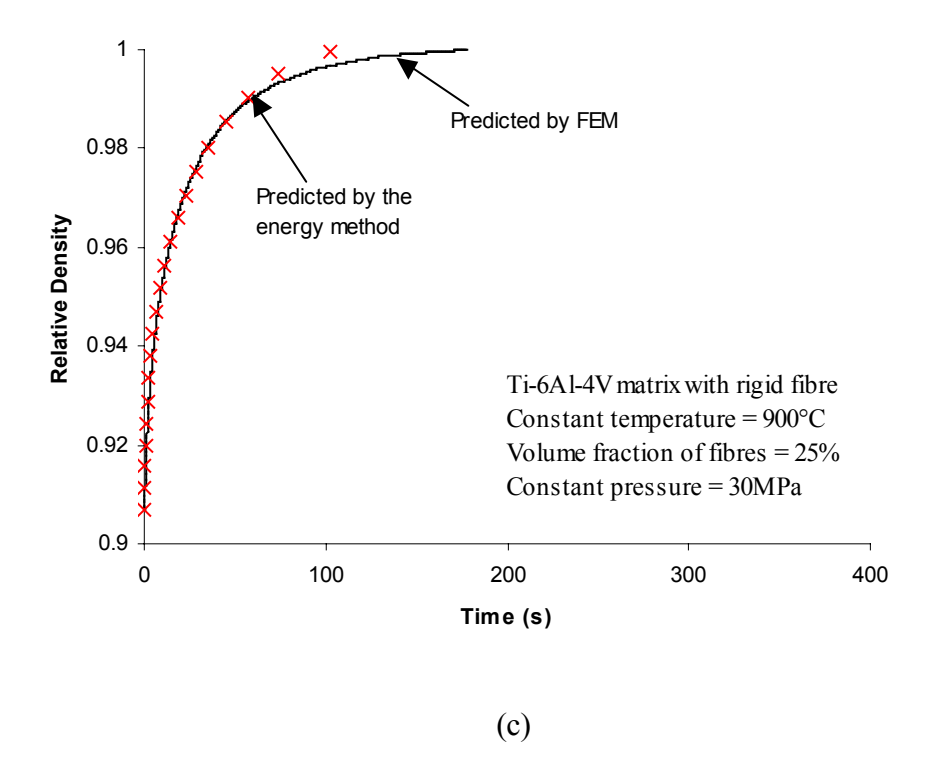


Figure 5 Graphs showing the variation of relative density with time at a constant temperature of 900°C for a range of constant pressures predicted (a) by the energy method and (b) by the finite element model.







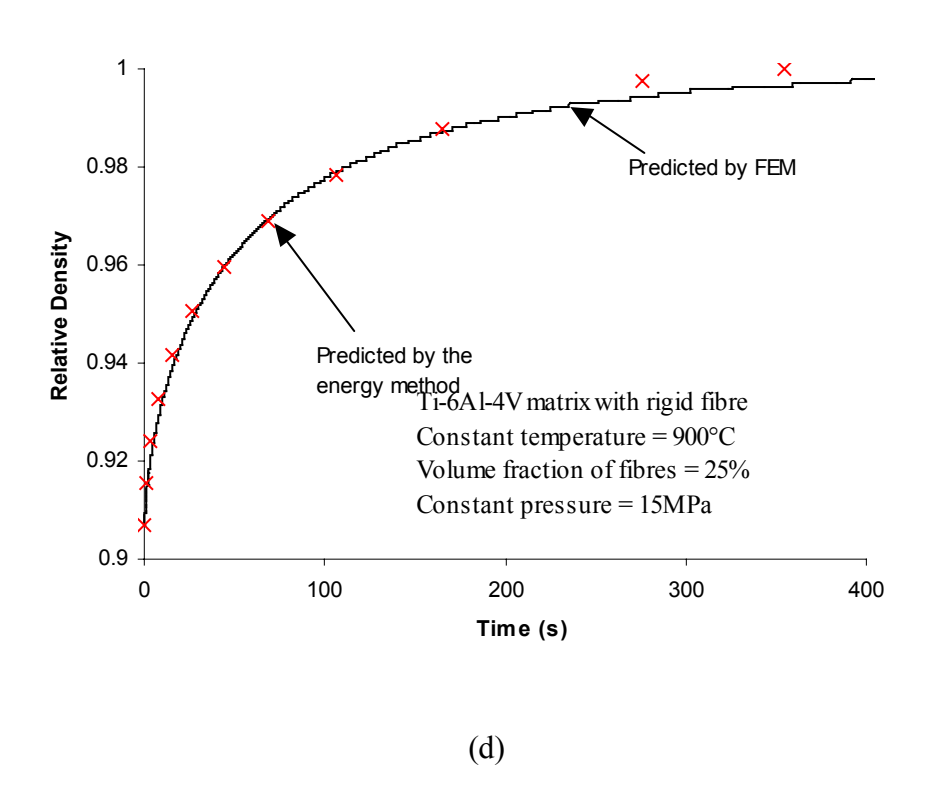


Figure 6 Graph showing direct comparisons of the variation of relative density with time curves predicted by the energy method and the finite element model for a range of applied pressures.

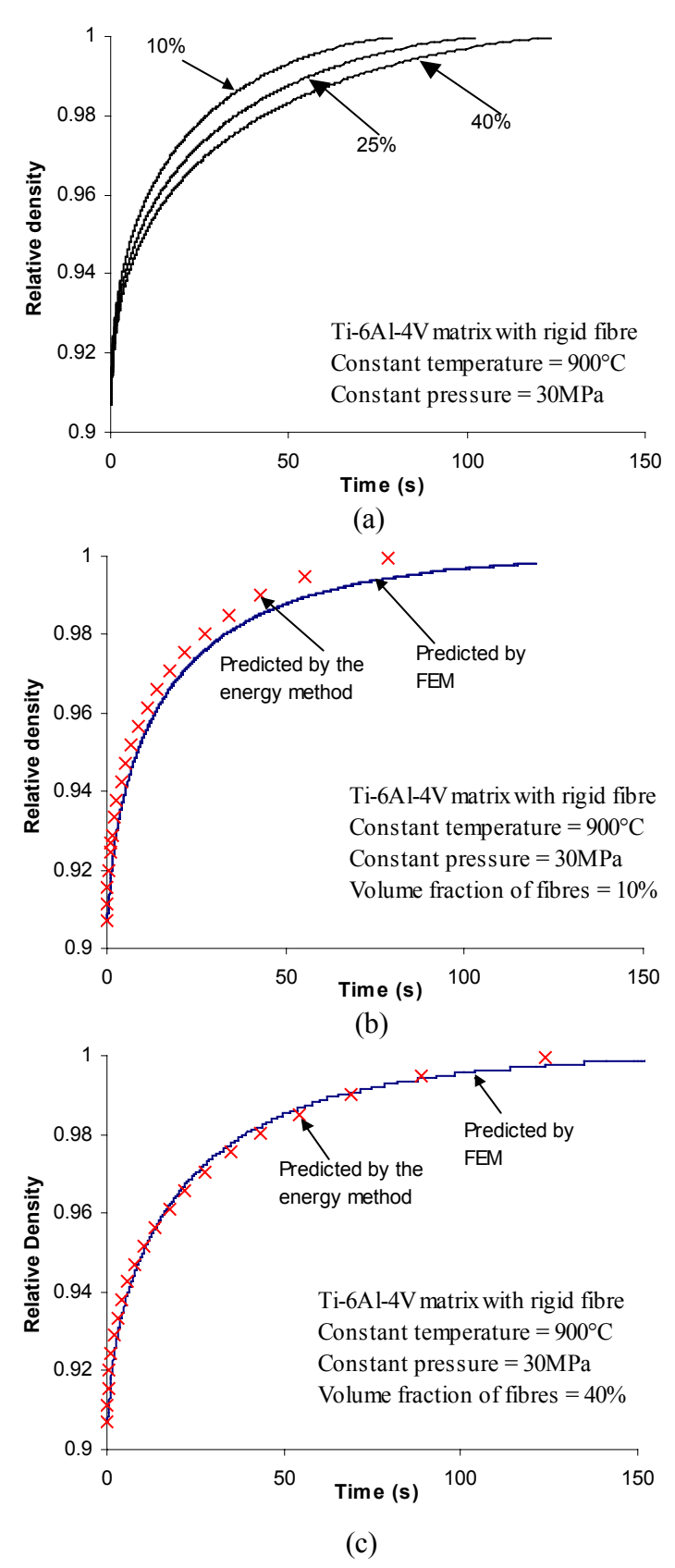


Figure 7 Graphs showing the variation of relative density with time (a) predicted by the energy method for a range of volume fractions of fibres at 900°C, (b) predicted by the energy method and the finite element model for 40% volume fraction of fibres and (c) predicted by the energy method and the finite element model for 10% volume fraction of fibres.

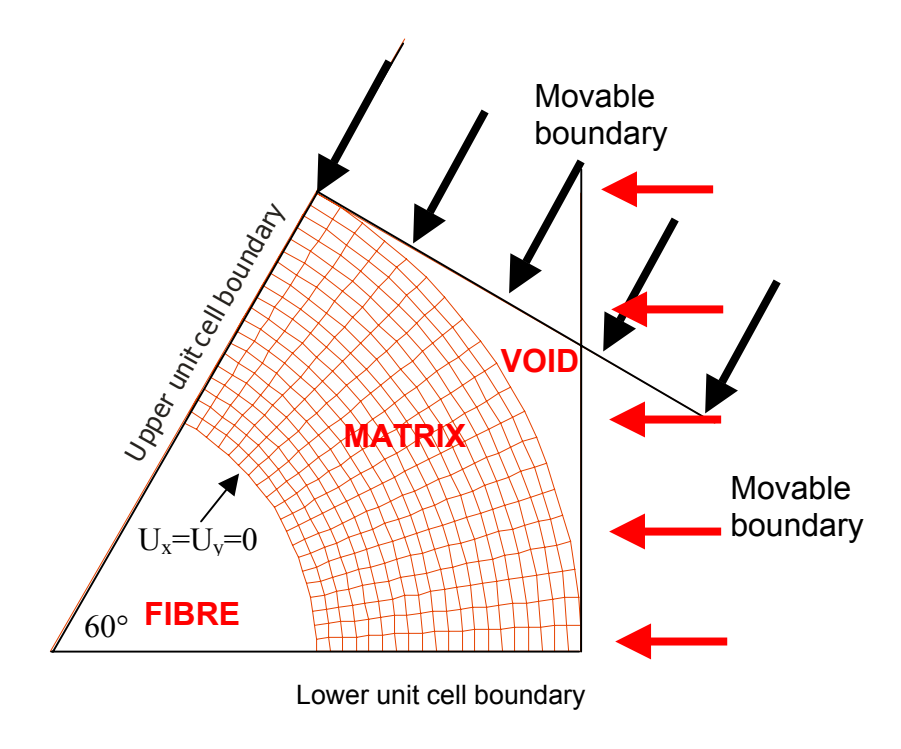


Figure 8 Schematic diagram showing the micromechanical finite element model for asymmetric pressure application

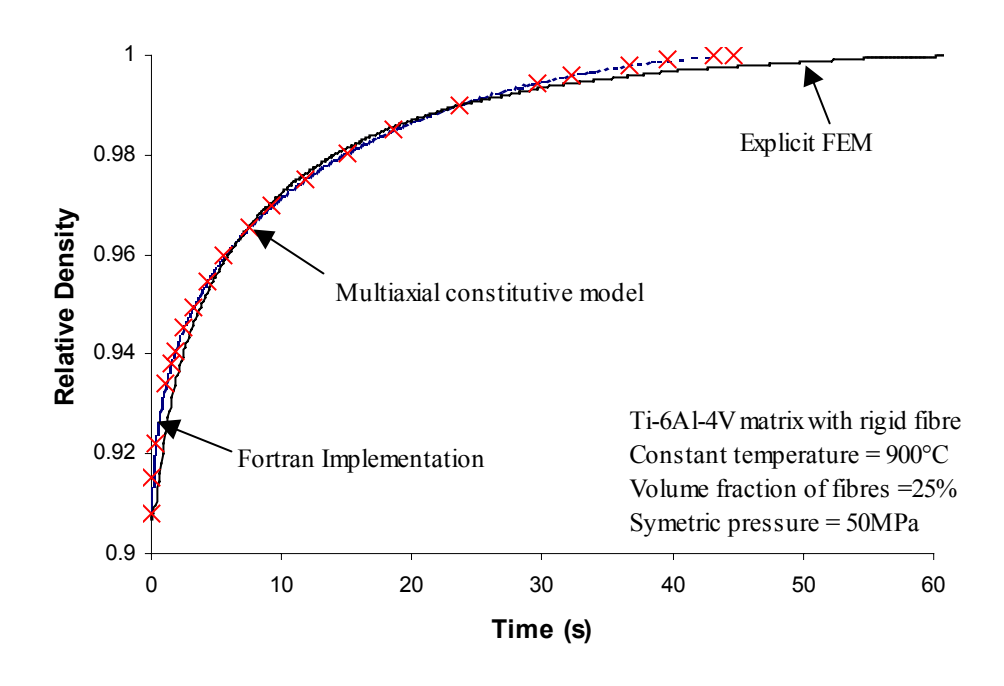


Figure 9 Comparisons of relative density evolution with time obtained from the multiaxial constitutive model, the explicit finite element model and fortran implementation at constant temperature of 900°C, 25% volume fraction of fibres and with symmetric pressure of 50MPa.

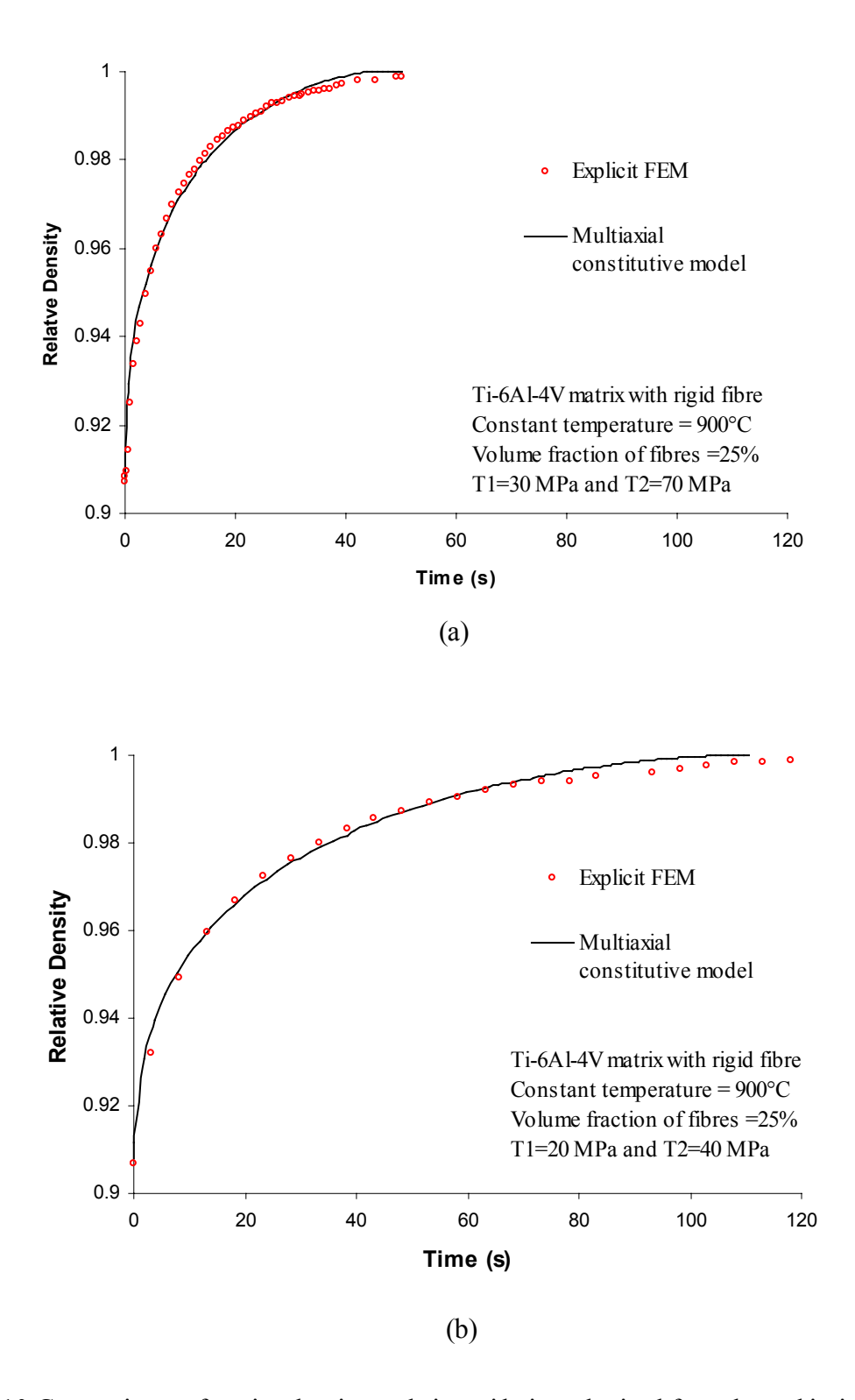


Figure 10 Comparisons of reative density evolution with time obtained from the multiaxial constitutive model and the explicit finite element model at constant temperature of 900°C, 25% volume fraction of fibres and for (a) T1=30 MPa, T2=70 MPa and (b) T1=20 MPa, T2=40 MPa.

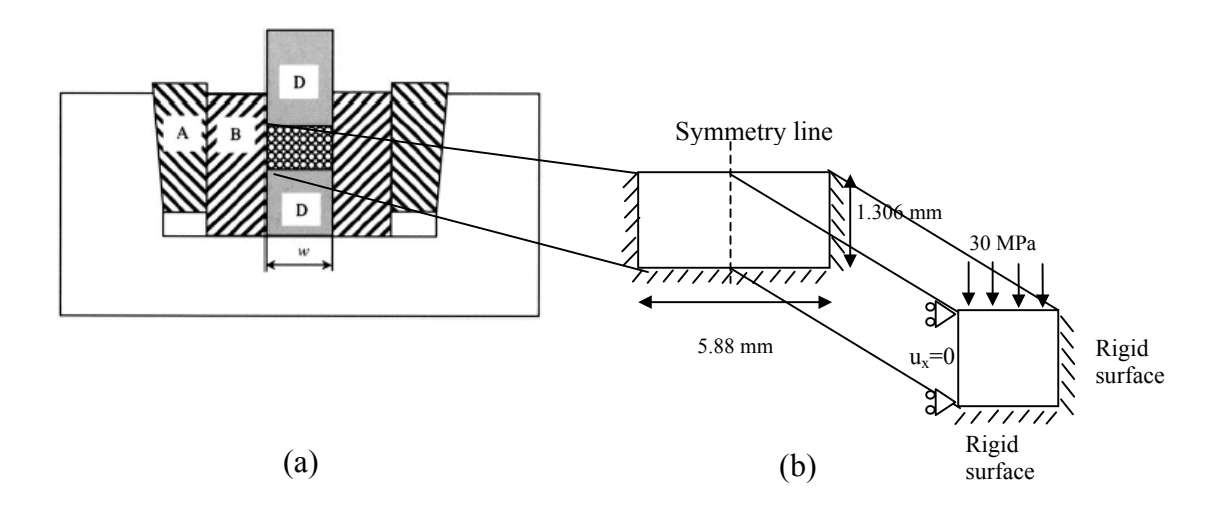


Figure 11 Schematic diagrams showing (a) the experimental set up (taken from Peng et al. 2005) and (b) the finite element model.

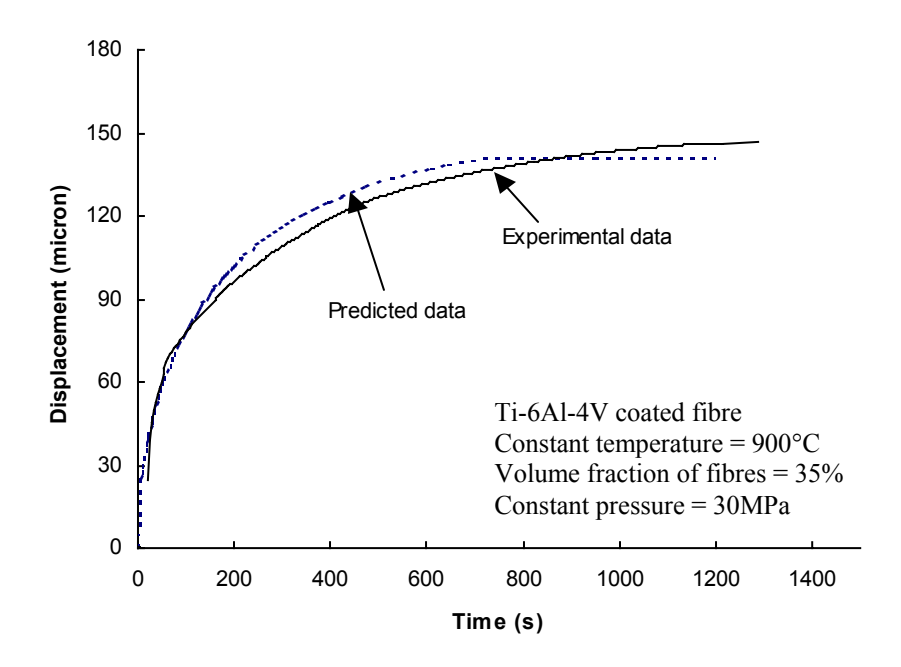


Figure 12 graph showing a comparison of predicted and experimental displacement versus time curves for a hexagonal fibre array under constrained uniaxial hot pressing at 900°C and 30 MPa

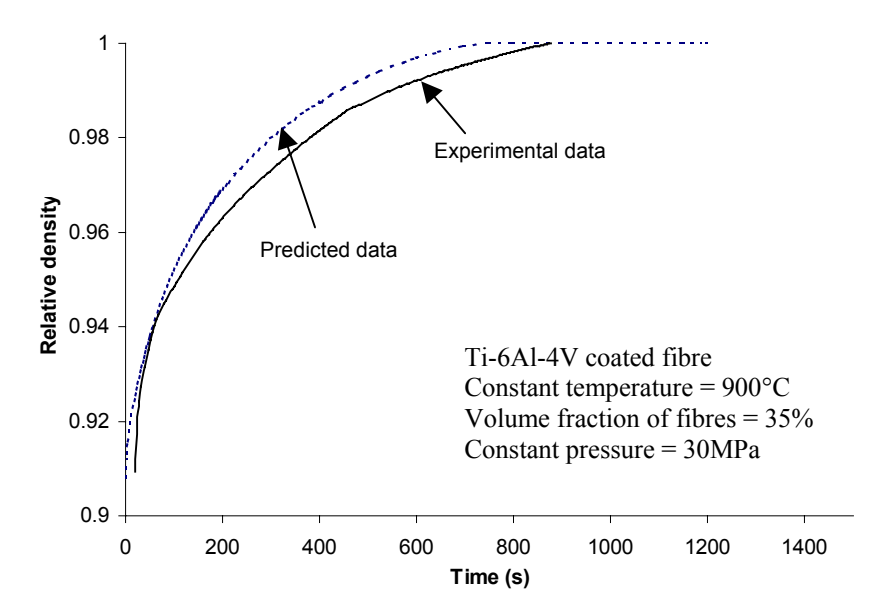


Figure 13 Graph showing a comparison of predicted and experimental densification curves for a hexagonal fibre array under constrained uniaxial hot pressing at 900°C and 30 MPa

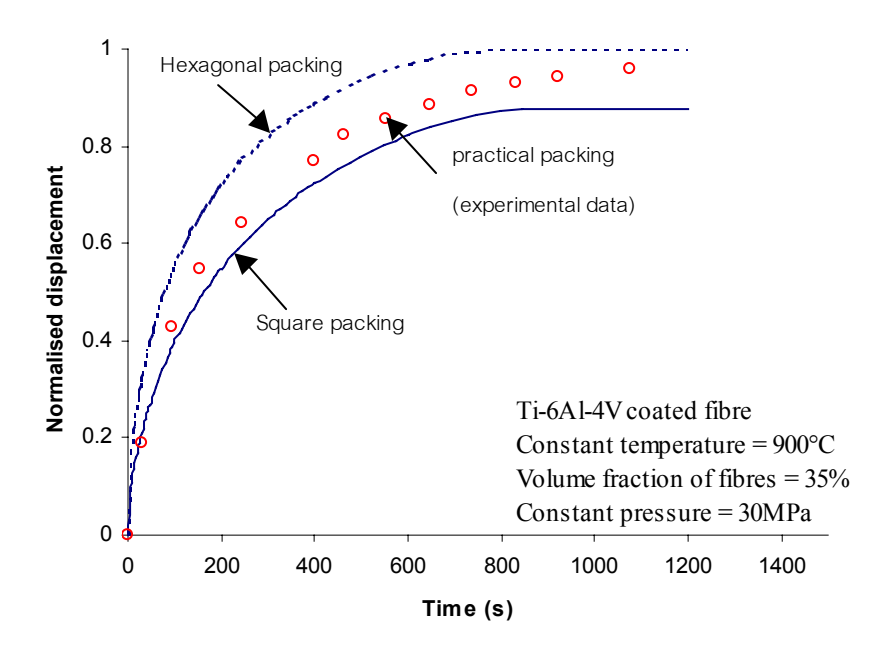


Figure 14 Graph showing a comparison of normalised displacement versus time curves obtained from a practical consolidation process, simulations with square array and hexagonal array packing of coated fibres.

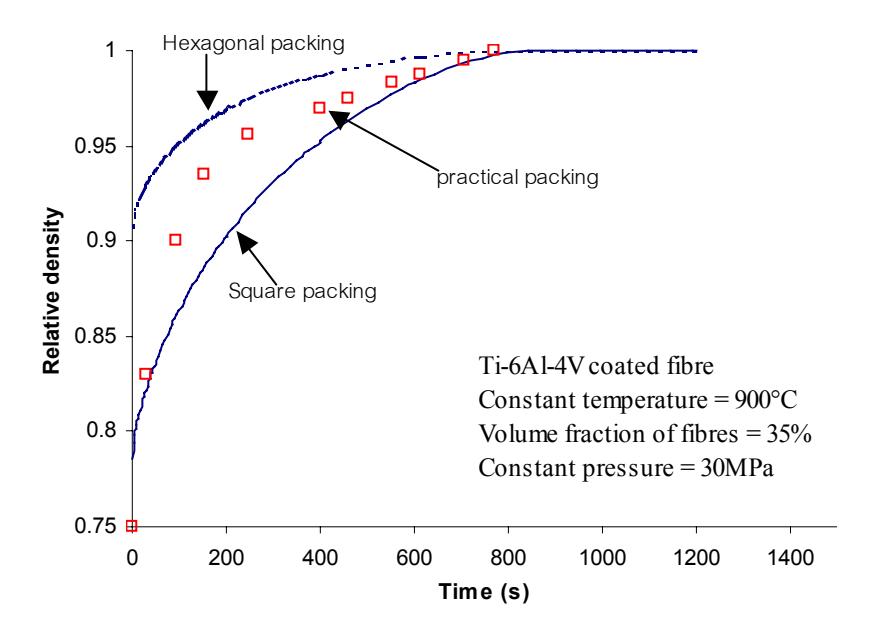


Figure 15 Graph showing densification curves for consolidation of both hexagonal and square array packing of coated fibres under constrained uniaxial hot pressing which provide the upper and lower bounds for a practical process as illustrated by the square symbol.

# ผลลัพธ์จากโครงการวิจัยที่ได้รับทุนจาก สกว.

ทำการส่งบทความวิจัยเรื่อง Hexagonal array matrix-coated fibre composite consolidation model เพื่อตี พิมพ์ในวารสารวิชาการนานาชาติ Journal of Materials Research

# ภาคผนวก